

LA-UR- 03-2983

Approved for public release;
distribution is unlimited.

72

Title: MINIBOONE

Author(s): WILLIAM C. LOUIS, LANL, P-25

Submitted to: Proceedings Publication for:
10TH INTERNATIONAL WORKSHOP ON:
"NEUTRINO TELESCOPES"
March 11-13, 2003
Venice, Italy



Los Alamos National Laboratory, an affirmative action/equal opportunity employer, is operated by the University of California for the U.S. Department of Energy under contract W-7405-ENG-36. By acceptance of this article, the publisher recognizes that the U.S. Government retains a nonexclusive, royalty-free license to publish or reproduce the published form of this contribution, or to allow others to do so, for U.S. Government purposes. Los Alamos National Laboratory requests that the publisher identify this article as work performed under the auspices of the U.S. Department of Energy. Los Alamos National Laboratory strongly supports academic freedom and a researcher's right to publish; as an institution, however, the Laboratory does not endorse the viewpoint of a publication or guarantee its technical correctness.

MINIBOONE

W. C. LOUIS for the MiniBooNE collaboration ¹⁾
Physics Division, Los Alamos National Laboratory,
Los Alamos, NM 87545, USA
E-mail: louis@lanl.gov

ABSTRACT

Employing 800 MeV, high-intensity proton beams, the LSND and KARMEN experiments have performed sensitive searches for neutrino oscillations. Whereas LSND observes evidence for neutrino oscillations with $\Delta m^2 > 0.2 \text{ eV}^2$, KARMEN sees no such evidence. However, a joint analysis of the two experiments shows that the data sets are compatible with oscillations occurring either in a band from 0.2 to 1 eV^2 or in a region around 7 eV^2 . The MiniBooNE experiment, which has recently become operational at Fermilab, will be a definitive test of the LSND evidence for neutrino oscillations and will be capable of making a precision measurement of the oscillation parameters and of searching for CP and CPT violation in the lepton sector.

1. Introduction

The LSND ²⁾ and KARMEN ³⁾ experiments were designed to search for $\bar{\nu}_\mu \rightarrow \bar{\nu}_e$ oscillations with high sensitivity and to measure νC cross sections. A comparison of the two experiments is given in Table 1. LSND had the advantage of a higher proton intensity, a larger detector mass, and good particle identification, while KARMEN had a lower duty factor and excellent energy resolution. An important difference between the experiments is that the LSND neutrino distance was 30 m, compared to 17.7 m for KARMEN, so that a combined analysis provides a more sensitive search for neutrino oscillations. Both experiments made use of a high-intensity, 800 MeV proton beam that interacted in an absorber to produce a large number of pions. Most of the pions produced are π^+ , which almost all decay. The π^- are mainly absorbed and only a small fraction decay to μ^- , which in turn are largely captured. Therefore, almost all of the neutrinos produced arise from $\pi^+ \rightarrow \mu^+ \nu_\mu$ and $\mu^+ \rightarrow e^+ \bar{\nu}_\mu \nu_e$ decays, where most of the decays ($> 95\%$) are at rest and only a small fraction ($< 5\%$) are in flight. After six years of data collection, the LSND experiment obtained evidence for neutrino oscillations in the mass range $\Delta m^2 > 0.2 \text{ eV}^2$. Although this evidence was not confirmed by the KARMEN experiment, a joint analysis of the two experiments ⁴⁾ reveals regions of compatibility in a band from 0.2 to 1 eV^2 and in a region around 7 eV^2 .

The MiniBooNE experiment at Fermilab ⁵⁾ is designed to provide a definitive test of the LSND evidence for neutrino oscillations and is beginning to take data. The MiniBooNE detector consists of a 12.2 m diameter sphere filled with oil and covered on the inside by 1520 phototubes (PMTs), 1280 of which are detector PMTs and 240 are veto PMTs. The detector is located approximately 500 m from the neutrino source,

Table 1: A comparison of the LSND and KARMEN experiments.

Property	LSND	KARMEN
Proton Energy	798 MeV	800 MeV
Proton Intensity	1000 μ A	200 μ A
Protons on Target	28,896 C	9425 C
Duty Factor	6×10^{-2}	1×10^{-5}
Total Mass	167 t	56 t
Neutrino Distance	30 m	17.7 m
Particle Identification	YES	NO
Energy Resolution at 50 MeV	6.6%	1.6%
Events for 100% $\bar{\nu}_\mu \rightarrow \bar{\nu}_e$ Transmutation	33,300	14,000

which is fed by the 8 GeV Booster operating at a current of 4 μ A. MiniBooNE will search for $\nu_\mu \rightarrow \nu_e$ oscillations from pion decay in flight (DIF) and will be capable of making precision measurements of the oscillation parameters and of searching for CP and CPT violation in the lepton sector. If neutrino oscillations are indeed observed, then the next phase of the experiment, BooNE, will be the construction of a second detector at a different distance, which will greatly improve the determination of the oscillation parameters.

2. LSND

2.1. Description of the Experiment

The LSND experiment ⁶⁾ was designed to search for $\bar{\nu}_\mu \rightarrow \bar{\nu}_e$ oscillations from μ^+ decay at rest (DAR) with high sensitivity. The LANSCE accelerator is an intense source of low energy neutrinos produced with a proton current of 1 mA at 798 MeV kinetic energy. For the 1993-1995 running period the production target consisted of a 30-cm long water target (20-cm in 1993) followed by a water-cooled Cu beam dump, while for the 1996-1998 running period the production target was reconfigured with the water target replaced by a close-packed, high-Z target. The resulting DAR neutrino fluxes are well understood because almost all detectable neutrinos arise from π^+ or μ^+ decay; π^- and μ^- that stop are readily captured in the Fe of the shielding and Cu of the beam stop ⁷⁾. The production of kaons or heavier mesons is negligible at these proton energies. The $\bar{\nu}_e$ flux is calculated to be only $\sim 8 \times 10^{-4}$ as large as the $\bar{\nu}_\mu$ flux in the $20 < E_\nu < 52.8$ MeV energy range, so that the observation of a $\bar{\nu}_e$ event rate significantly above the calculated background would be evidence for $\bar{\nu}_\mu \rightarrow \bar{\nu}_e$ oscillations. Fig. 1 shows the neutrino energy spectra from π^+ and μ^+ DAR.

The LSND detector ⁶⁾ consisted of an approximately cylindrical tank 8.3 m long by 5.7 m in diameter. A schematic drawing of the detector is shown in Fig. 2. The center of the detector was 30 m from the neutrino source. On the inside surface of the

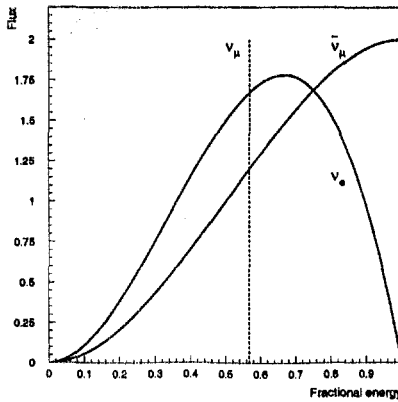


Figure 1: The neutrino energy spectra from π^+ and μ^+ DAR.

tank, 1220 8-inch Hamamatsu PMTs covered 25% of the area with photocathode. The tank was filled with 167 t of liquid scintillator consisting of mineral oil and 0.031 g/l of b-PBD. This low scintillator concentration allows the detection of both Čerenkov light and scintillation light and yields an attenuation length of more than 20 m for wavelengths greater than 400 nm ⁸⁾. A typical 45 MeV electron created in the detector produced a total of ~ 1500 photoelectrons, of which ~ 280 photoelectrons were in the Čerenkov cone. PMT time and pulse-height signals were used to reconstruct the track with an average RMS position resolution of ~ 14 cm, an angular resolution of $\sim 12^\circ$, and an energy resolution of $\sim 7\%$ at the Michel endpoint of 52.8 MeV. The Čerenkov cone for relativistic particles and the time distribution of the light, which is broader for non-relativistic particles ⁶⁾, gave excellent separation between electrons and particles below Čerenkov threshold. Identification of neutrons was accomplished through the detection of the 2.2 MeV γ from neutron capture on a free proton. The veto shield enclosed the detector on all sides except the bottom. Additional counters were placed below the veto shield after the 1993 run to reduce cosmic-ray background entering through the bottom support structure. The main veto shield ⁹⁾ consisted of a 15-cm layer of liquid scintillator in an external tank and 15 cm of lead shot in an internal tank. This combination of active and passive shielding tagged cosmic-ray muons that stopped in the lead shot. A veto inefficiency $< 10^{-5}$ was achieved for incident charged particles.

2.2. Event Selection

The goal of the event selection is to reduce the cosmic-ray background to as low a level as possible, while retaining a high efficiency for neutrino-induced electron events. The selection criteria and corresponding efficiencies are shown in Table 2.

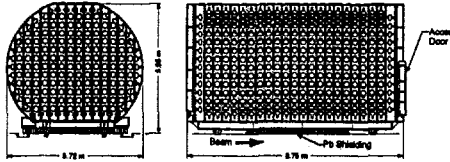


Figure 2: A schematic drawing of the LSND detector.

The energy range $20 < E < 200$ MeV is chosen so as to accept both DAR $\bar{\nu}_\mu \rightarrow \bar{\nu}_e$ and DIF $\nu_\mu \rightarrow \nu_e$ oscillation candidates. $20 < E_e < 60$ MeV is required for the $\bar{\nu}_\mu \rightarrow \bar{\nu}_e$ oscillation search and $60 < E_e < 200$ MeV for the $\nu_\mu \rightarrow \nu_e$ oscillation search. Below 20 MeV there are large backgrounds from the β decay of ^{12}B created by the capture of stopped cosmic-ray μ^- on ^{12}C . Above 200 MeV the beam-related backgrounds from $\pi^+ \rightarrow e^+\nu_e$ are large compared to any likely oscillation signal. Events with a previous activity within $12 \mu\text{s}$, a future activity within $8 \mu\text{s}$, or a bottom veto counter hit are rejected in order to eliminate cosmic-ray muon events. To further minimize cosmic-ray background, a tight electron particle identification is applied, $-1.5 < \chi'_{tot} < 0.5$, where the allowed range is chosen by maximizing the selection efficiency divided by the square root of the beam-off background with a correlated neutron. The χ'_{tot} parameter depends on the product of the χ parameters defined in ⁶⁾. Briefly, χ_r and χ_a are the quantities minimized for the determination of the event position and direction, and χ_t is the fraction of PMT hits that occur more than 12 ns after the fitted event time. The dependence of the χ parameters on energy and position for Michel electrons was studied, and a correction was developed that made χ'_{tot} independent of energy or position. Additionally, no veto hit is allowed within 30 ns of the trigger time and the reconstructed electron vertex is required to be inside a volume 35 cm from the faces of the photomultiplier tubes. Finally, the number of associated γ s with $R_\gamma > 10$ (R_γ is discussed below) is required to be < 2 (> 1) for events < 60 (> 60) MeV in order to reject neutron-induced events, which tend to have many associated γ s. In addition to the electron reduction and selection efficiencies, Table 2 also shows the efficiencies due to the data acquisition (DAQ) and veto deadtime. The total efficiency for electrons in the fiducial volume with energies in the range $20 < E_e < 60$ MeV is 0.42 ± 0.03 .

Correlated 2.2 MeV γ from neutron capture are distinguished from accidental γ from radioactivity by use of the likelihood ratio, R_γ , which is defined to be the likelihood that the γ is correlated divided by the likelihood that the γ is accidental. R_γ depends on three quantities: the number of hit PMTs associated with the γ (the multiplicity is proportional to the γ energy), the distance between the reconstructed γ position and positron position, and the time interval between the γ and positron (neutrons have a capture time in mineral oil of $186 \mu\text{s}$, while the accidental γ are uniform in time). Fig. 3 shows these distributions, which are obtained from fits to the

Table 2: The LSND average efficiencies for electrons in the fiducial volume with energies in the range $20 < E_e < 60$ MeV.

Criteria	Efficiency
Electron Reduction	
Veto Hits < 4	0.98 ± 0.01
Loose Electron PID	0.96 ± 0.01
Cosmic Muon Cut	0.92 ± 0.01
Electron Selection	
$\Delta t_{past} > 12\mu s$	0.96 ± 0.01
$\Delta t_{future} > 8\mu s$	0.99 ± 0.01
$-1.5 < \chi'_{tot} < 0.5$	0.84 ± 0.01
$0.3 < \chi_{tot}^{old} < 0.65$ (1993 only)	0.98 ± 0.01
$\Delta t_{veto}^{best} > 30ns$	0.97 ± 0.01
$D > 35$ cm	0.88 ± 0.02
$N_\gamma < 1, E > 60$	1.00
$N_\gamma < 2, E < 60$	1.00
Deadtime	
DAQ & Tape Deadtime	0.96 ± 0.02
Veto Deadtime	0.76 ± 0.02
Total	0.42 ± 0.03

data, for both correlated 2.2 MeV γ (solid curves) and accidental γ (dashed curves). To determine R_γ , the product of probabilities for the correlated distributions is formed and divided by the product of probabilities for the uncorrelated distributions. The accidental γ efficiencies are measured from the laser-induced calibration events, while the correlated γ efficiencies are determined from the Monte Carlo simulation of the experiment. Similar results for the correlated γ efficiencies are obtained from the cosmic-ray neutron events, whose high energy give them a slightly broader position distribution. The systematic uncertainty of these efficiencies is estimated to be $\pm 7\%$ of their values. For $R_\gamma > 10$, the correlated and accidental efficiencies are 0.39 and 0.003, respectively.

2.3. Neutrino Oscillation Signal and Background Reactions

The primary oscillation search in LSND is for $\bar{\nu}_\mu \rightarrow \bar{\nu}_e$ oscillations, where the $\bar{\nu}_\mu$ arise from μ^+ DAR in the beam stop and the $\bar{\nu}_e$ are identified through the reaction $\bar{\nu}_e p \rightarrow e^+ n$. This reaction allows a two-fold signature of a positron with a 52.8 MeV endpoint and a correlated 2.2 MeV γ from neutron capture on a free proton. There are only two significant neutrino backgrounds with a positron/electron and a correlated neutron. The first background is from μ^- DAR in the beam stop followed by $\bar{\nu}_e p \rightarrow e^+ n$ scattering in the detector. As mentioned earlier, this background is highly suppressed due to the requirements that a π^- be produced, the π^- DIF, and

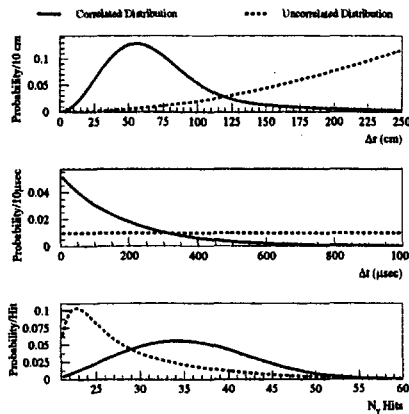


Figure 3: Distributions for correlated 2.2 MeV γ (solid curves) and accidental γ (dashed curves) from LSND. The top plot shows the distance between the reconstructed γ position and positron position, $\Delta\tau$, the middle plot shows the time interval between the γ and positron, Δt , and the bottom plot shows the number of hit PMTs associated with the γ , N_{hits} .

Table 3: The LSND estimated number of events in the $20 < E_e < 60$ MeV energy range due to 100% $\bar{\nu}_\mu \rightarrow \bar{\nu}_e$ transmutation and to the two beam-related backgrounds with neutrons, μ^- DAR in the beam stop followed by $\bar{\nu}_e p \rightarrow e^+ n$ scattering in the detector and π^- DIF in the beam stop followed by $\bar{\nu}_\mu p \rightarrow \mu^+ n$ scattering. The events must satisfy the electron selection criteria, but no correlated γ requirement is imposed.

Neutrino Source	Reaction	Number of Events
μ^+ DAR	100% $\bar{\nu}_\mu \rightarrow \bar{\nu}_e$	33300 ± 3300
μ^- DAR	$\bar{\nu}_e p \rightarrow e^+ n$	19.5 ± 3.9
π^- DIF	$\bar{\nu}_\mu p \rightarrow \mu^+ n$	10.5 ± 4.6

the μ^- DAR prior to capture. The second background is from π^- DIF in the beam stop followed by $\bar{\nu}_\mu p \rightarrow \mu^+ n$ scattering in the detector. (Additional contributions are from $\bar{\nu}_\mu C \rightarrow \mu^+ n X$ and $\nu_\mu C \rightarrow \mu^- n X$ scattering.) This background will mimic the oscillation reaction if the μ^+ is sufficiently low in energy that it is below the threshold of 18 hit PMTs, corresponding to $E_\mu < 4$ MeV. Table 3 shows the estimated number of events in the $20 < E_e < 60$ MeV energy range satisfying the electron selection criteria for 100% $\bar{\nu}_\mu \rightarrow \bar{\nu}_e$ transmutation and for the two beam-related backgrounds with neutrons.

2.4. Neutrino Oscillation Results

Table 4 shows the statistics for events that satisfy the selection criteria for the primary $\bar{\nu}_\mu \rightarrow \bar{\nu}_e$ oscillation search. An excess of events is observed over that expected from beam-off and neutrino background that is consistent with neutrino oscillations.

Table 4: Numbers of LSND beam-on events that satisfy the selection criteria for the primary $\bar{\nu}_\mu \rightarrow \bar{\nu}_e$ oscillation search with $R_\gamma > 1$, $R_\gamma > 10$, and $R_\gamma > 100$. Also shown are the beam-off background, the estimated neutrino background, and the excess of events that is consistent with neutrino oscillations.

Selection	Beam-On Events	Beam-Off Background	ν Background	Event Excess
$R_\gamma > 1$	205	106.8 ± 2.5	39.2 ± 3.1	$59.0 \pm 14.5 \pm 3.1$
$R_\gamma > 10$	86	36.9 ± 1.5	16.9 ± 2.3	$32.2 \pm 9.4 \pm 2.3$
$R_\gamma > 100$	27	8.3 ± 0.7	5.4 ± 1.0	$13.3 \pm 5.2 \pm 1.0$

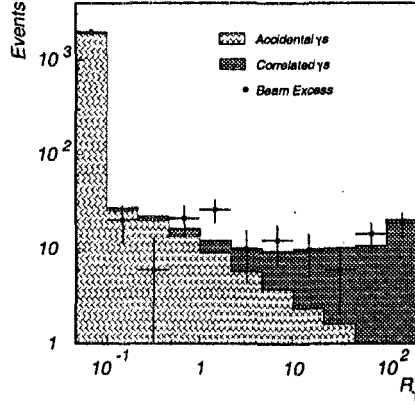


Figure 4: The LSND R_γ distribution for events that satisfy the selection criteria for the primary $\bar{\nu}_\mu \rightarrow \bar{\nu}_e$ oscillation search.

A χ^2 fit to the R_γ distribution, as shown in Fig. 4, gives $f_c = 0.0567 \pm 0.0108$ ($\chi^2 = 10.7/9$ DOF), which leads to a beam on-off excess of 117.9 ± 22.4 events with a correlated neutron. Subtracting the neutrino background from μ^- DAR followed by $\bar{\nu}_e p \rightarrow e^+ n$ scattering (19.5 ± 3.9 events) and π^- DIF followed by $\bar{\nu}_\mu p \rightarrow \mu^+ n$ scattering (10.5 ± 4.6 events)¹⁰ leads to a total excess of $87.9 \pm 22.4 \pm 6.0$ events. This excess corresponds to an oscillation probability of $(0.264 \pm 0.067 \pm 0.045)\%$, where the first error is statistical and the second error is the systematic error arising from uncertainties in the backgrounds, neutrino flux (7%), e^+ efficiency (7%), and γ efficiency (7%).

A clean sample of oscillation candidate events can be obtained by requiring $R_\gamma > 10$, where as shown in Table 4, the beam on-off excess is 49.1 ± 9.4 events while the estimated neutrino background is only 16.9 ± 2.3 events. Fig. 5 displays the energy distribution of events with $R_\gamma > 10$. The shaded regions show the combination of neutrino background plus neutrino oscillations at low Δm^2 . The data agree well with the oscillation hypothesis. Fig. 6 shows the spatial distribution for events with $R_\gamma > 10$ and $20 < E_e < 60$ MeV, where z is along the axis of the tank (and approximately along the beam direction), y is vertical, and x is transverse. The shaded

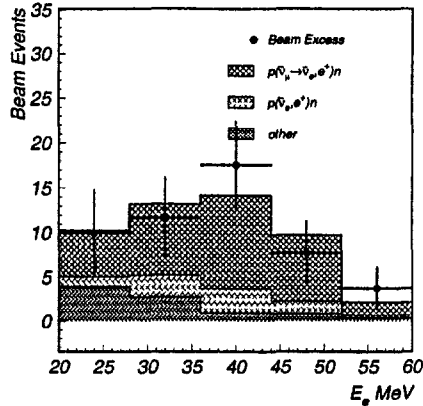


Figure 5: The LSND energy distribution for events with $R_\gamma > 10$. The shaded region shows the expected distribution from a combination of neutrino background plus neutrino oscillations at low Δm^2 .

region shows the expected distribution from a combination of neutrino background plus neutrino oscillations. Finally, Fig. 7 shows the L_ν/E_ν distribution for events with $R_\gamma > 10$ and $20 < E_e < 60$ MeV, where L_ν is the distance travelled by the neutrino in meters and E_ν is the neutrino energy in MeV determined from the measured positron energy and angle with respect to the neutrino beam. The data agree well with the expectation from neutrino background plus neutrino oscillations at low Δm^2 ($\chi^2 = 4.9/8$ D.O.F.) or high Δm^2 ($\chi^2 = 5.8/8$ D.O.F.).

The $(\sin^2 2\theta, \Delta m^2)$ likelihood (\mathcal{L}) fitter is applied to beam-on events in the final oscillation sample and calculates a likelihood in the $(\sin^2 2\theta, \Delta m^2)$ plane in order to extract the favored oscillation parameters. The \mathcal{L} product in the $(\sin^2 2\theta, \Delta m^2)$ plane is formed over the individual beam-on events that pass the oscillation cuts. This three-dimensional contour is sliced to arrive finally at the LSND allowed oscillation region. The beam-related backgrounds are determined from MC event samples for each individual background contribution. The MC contains the trigger simulation and generally very well reproduces the tank response to all particles of interest. Agreement between the data and MC is excellent.

The $(\sin^2 2\theta, \Delta m^2)$ oscillation parameter fit for the entire data sample, $20 < E_e < 200$ MeV, is shown in Fig. 8. The fit includes both $\bar{\nu}_\mu \rightarrow \bar{\nu}_e$ and $\nu_\mu \rightarrow \nu_e$ oscillations, as well as all known neutrino backgrounds. The inner and outer regions correspond to 90% and 99% CL allowed regions, while the curves are 90% CL limits from the Bugey reactor experiment ¹²⁾ and the KARMEN experiment at ISIS ³⁾. The most favored allowed region is the band from $0.2 - 2.0$ eV², although a region around 7 eV² is also possible.

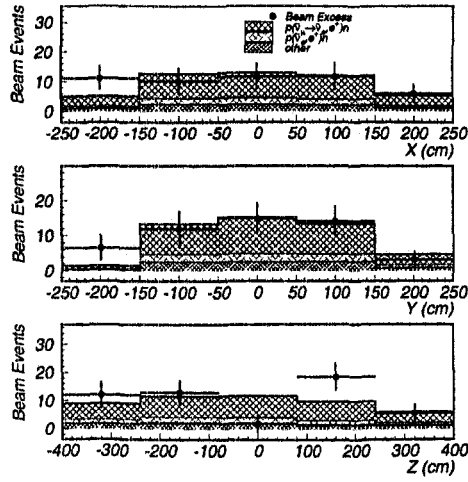


Figure 6: The LSND spatial distributions for events with $R_\gamma > 10$ and $20 < E_e < 60$ MeV. The shaded region shows the expected distribution from a combination of neutrino background plus neutrino oscillations at low Δm^2 .

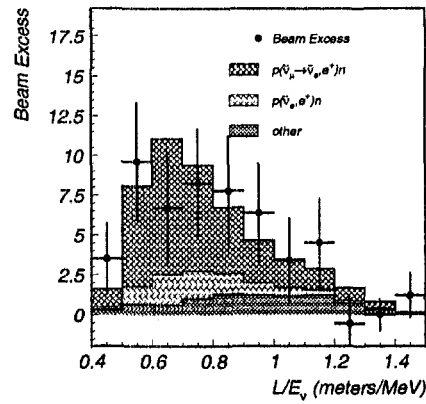


Figure 7: The LSND L_ν/E_ν distribution for events with $R_\gamma > 10$ and $20 < E_e < 60$ MeV, where L_ν is the distance travelled by the neutrino in meters and E_ν is the neutrino energy in MeV. The data agree well with the expectation from neutrino background and neutrino oscillations at low Δm^2 .

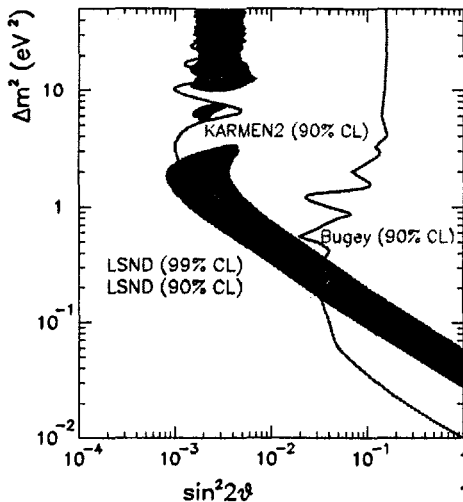


Figure 8: The $(\sin^2 2\theta, \Delta m^2)$ oscillation parameter fit for the entire LSND data sample, $20 < E_e < 200$ MeV. The inner and outer regions correspond to 90% and 99% CL allowed regions, while the curves are 90% CL limits from the Bugey reactor experiment and the KARMEN experiment at ISIS.

3. KARMEN

3.1. Description of the Experiment

The KARMEN experiment ¹³⁾ makes use of the ISIS rapid-cycling synchrotron, which accelerates protons up to 800 MeV at an intensity of 200 μ A. The protons are extracted from the synchrotron at a frequency of 50 Hz as a double pulse consisting of two 100 ns pulses separated by 325 ns. The two bursts, therefore, occur within 600 ns and lead to an overall duty factor of about 10^{-5} . After extraction, the protons interact in a water-cooled Ta-D₂O target, producing about (0.0448 ± 0.0030) π^+ per incident proton ⁷⁾. Due to the small duty factor, ν_μ from π^+ decay can be clearly separated from the $\bar{\nu}_\mu$ and ν_e from μ^+ decay. The $\bar{\nu}_e/\bar{\nu}_\mu$ background is estimated to be 6.4×10^{-4} ⁷⁾, slightly smaller than for LSND.

The KARMEN detector, as shown in Fig. 9, is a segmented, liquid scintillator calorimeter with 608 modules and a total mass of 56 t. The liquid scintillator is made of paraffin oil (75% vol.), pseudocumene (25% vol.), and PMP (2 g/l). The modules are read-out by pairs of 3" PMTs and are enclosed by a tank with outside dimensions 3.53 m x 3.20 m x 5.96 m. Excellent energy resolution is obtained for electrons produced inside the detector and can be parametrized by $\sigma_E = 11.5\%/\sqrt{E(\text{MeV})}$. Gadolinium-coated paper was inserted between the modules for the detection of thermal neutrons. The detector is enclosed by a multilayer active veto system and 7000 t

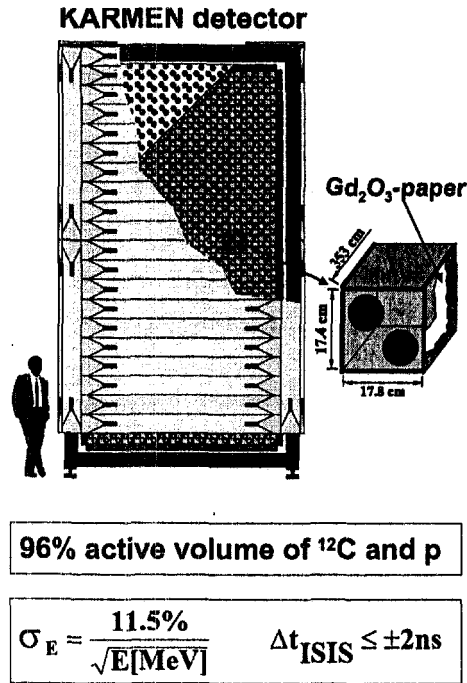


Figure 9: A schematic drawing of the KARMEN detector.

of steel shielding and is located 17.7 m from the neutrino source at an angle of 100° to the incident proton beam direction.

3.2. Event Selection

KARMEN searches for $\bar{\nu}_\mu \rightarrow \bar{\nu}_e$ oscillations in the same way as in LSND by looking for the reaction $\bar{\nu}_e p \rightarrow e^+ n$, which gives a two-fold signature of a e^+ followed by one or more γ from neutron capture. The neutrino oscillation event selection and corresponding efficiencies are summarized in Table 5. For the e^+ candidate it is required that there be no previous activity in the detector and veto, that the e^+ occur from $0.6\mu\text{s}$ to $10.6\mu\text{s}$ after the beam spill, and that the e^+ energy be in the range from 16 MeV to 50 MeV. For the γ candidate it is required that the γ occur from $5\mu\text{s}$ to $300\mu\text{s}$ after the e^+ , that the γ have an energy less than 8.0 MeV, and that the γ be reconstructed within a coincidence volume of 1.3 m^3 . The total efficiency for the two-fold signature is estimated to be 0.192 ± 0.0145 .

3.3. Neutrino Oscillation Signal and Background Reactions

Table 6 shows the estimated number of events in the $16 < E_e < 50$ MeV energy range for 100% $\bar{\nu}_\mu \rightarrow \bar{\nu}_e$ transmutation. Also shown are the number of events for the four backgrounds with apparent neutrons. The first background is the cosmic-

Table 5: The KARMEN event selection and corresponding efficiencies for the $\bar{\nu}_\mu \rightarrow \bar{\nu}_e$ oscillation search.

Event	Selection	Efficiency
e^+	no previous activity	0.709
e^+	$0.6 < t_{pr} < 300\mu s$	0.840
e^+	$16 < E_{pr} < 50 \text{ MeV}$	0.775
(n, γ)	$5 < \Delta t < 300\mu s$	0.416
(n, γ)	$E_{del} < 8.0 \text{ MeV}$	
(n, γ)	$V_c = 1.3m^3$	

Table 6: The KARMEN estimated number of events in the $16 < E_e < 50 \text{ MeV}$ energy range due to 100% $\bar{\nu}_\mu \rightarrow \bar{\nu}_e$ transmutation and to the four backgrounds with apparent neutrons.

Process	Number of Events
100% $\bar{\nu}_\mu \rightarrow \bar{\nu}_e$	5826 ± 534
Cosmic-induced Background	3.9 ± 0.2
Charged-current Coincidences	5.1 ± 0.2
ν_e -induced Random Coincidences	4.8 ± 0.3
Intrinsic $\bar{\nu}_e$ Background	2.0 ± 0.2

induced background, which is well measured from data collected with the beam off. The second background is due to $\nu_e C \rightarrow e^- N_{gs}$, where the N_{gs} β decay mimics the γ from neutron capture. The third background is due to normal $\nu_e C \rightarrow e^- N^*$ inclusive interactions with an accidental γ coincidence. The final background is due to the intrinsic $\bar{\nu}_e$ contamination in the beam from μ^- DAR. The total background is estimated to be 15.8 ± 0.5 events.

3.4. Neutrino Oscillation Results

KARMEN observes 15 events that pass the selection criteria discussed above, which is consistent with the estimated background of 15.8 ± 0.5 events. The energy, time, and spatial distributions for the 15 events are shown in Fig. 10. Also shown are the shapes of the expected backgrounds, which are in good agreement with the data. A maximum likelihood fit to the data is performed ³⁾ to obtain the 90% C.L. limits, as shown in Fig. 8. The LSND oscillation region with $\Delta m^2 > 10 \text{ eV}^2$ is ruled-out by the KARMEN data; however, the regions $< 2 \text{ eV}^2$ and around 7 eV^2 are compatible with the LSND oscillation evidence.

4. Joint Analysis of LSND and KARMEN Data

A joint analysis of the LSND and KARMEN experiments has been performed ⁴⁾ that is based on a frequentist approach following the suggestions of ¹⁴⁾. For both

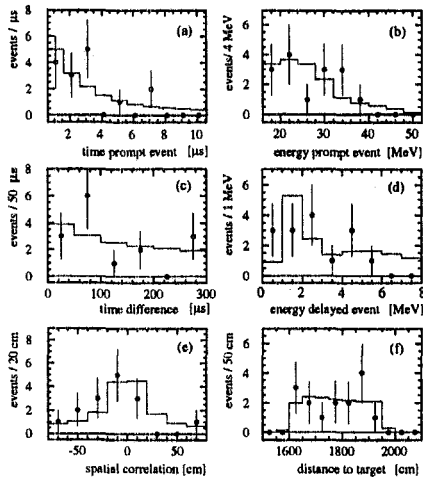


Figure 10: The energy, time, and spatial distributions for the events observed by the KARMEN experiment: (a) time of prompt events, (b) energy of prompt events, (c) time difference between prompt and delayed events, (d) energy of delayed events, (e) spatial correlation, and (f) distance to target of prompt events. The 15 oscillation candidate events are in good agreement with the background expectation of 15.8 events (solid line).

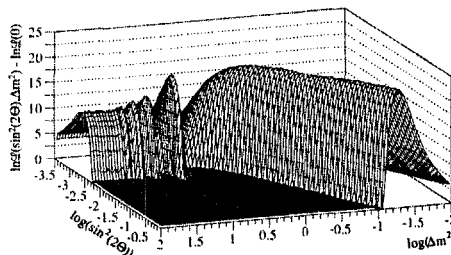


Figure 11: The combined LSND and KARMEN log-likelihood function in terms of $\sin^2 2\theta$ and Δm^2 .

experiments, the data are analyzed with a maximum likelihood analysis followed by the extraction of confidence levels in a unified approach. The two experiments are found to be incompatible at a level of combined confidence of 36%. For the cases of statistical compatibility, Fig. 11 shows the combined LSND and KARMEN log-likelihood function in terms of $\sin^2 2\theta$ and Δm^2 . The maximum log-likelihood function occurs at $\sin^2 2\theta = 1$ and $\Delta m^2 = 0.05 \text{ eV}^2$, which is 21.5 units of log-likelihood above the no oscillation hypothesis. Fig. 12 shows the confidence regions of the oscillation parameters for the combined likelihood analysis, assuming statistical compatibility of LSND and KARMEN. By combining the two experiments, the solutions with $\Delta m^2 > 10 \text{ eV}^2$ are excluded, and there remain essentially two solutions: one with $\Delta m^2 < 1 \text{ eV}^2$ and the other with $\Delta m^2 \sim 7 \text{ eV}^2$.

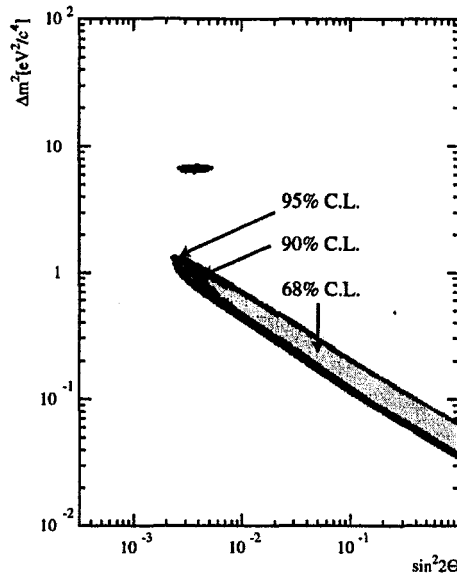


Figure 12: The confidence regions of the oscillation parameters for the combined likelihood analysis, assuming statistical compatibility of LSND and KARMEN.

5. MiniBooNE

5.1. Description of the Experiment

The MiniBooNE experiment is designed to be a definitive test of the LSND evidence for neutrino oscillations. The detector consists of a spherical tank 6.1 m (20 feet) in radius, as shown in Fig. 13, that stands in a 45-foot diameter cylindrical vault. An inner tank structure at 5.75 m radius supports 1280 8-inch PMTs (10% coverage) pointed inward and optically isolated from the outer region of the tank. The tank is filled with 800 t of mineral oil, resulting in a 500 t fiducial volume. The oil has a density of 0.836 and an index of refraction of 1.46. Even though the detector is filled with pure mineral oil, both Čerenkov and scintillation light are produced by particles in the oil. For $\beta = 1$ particles, about 5 photoelectrons are detected by the PMTs per MeV of energy loss. The scintillation light has an exponential time distribution with a time constant of ~ 18 ns. The measured amount of Čerenkov and scintillation light allows a rough determination of the energy deposited by particles above and below Čerenkov threshold.

The outer tank volume serves as a veto shield for identifying particles both entering and leaving the detector with 240 PMTs mounted near the tank wall. Above the detector tank is an electronics enclosure that houses the fast electronics and data

MiniBooNE Detector

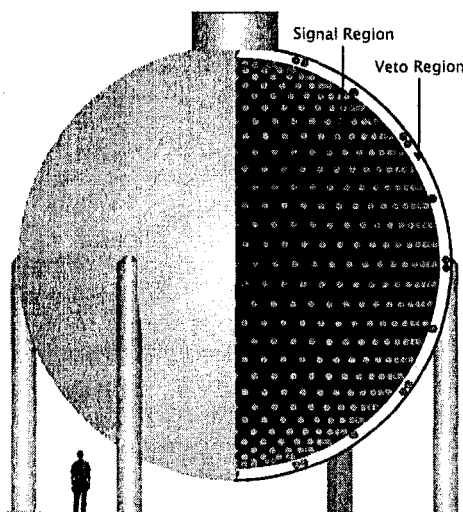


Figure 13: A schematic drawing of the MiniBooNE detector.

acquisition system and a utilities enclosure that houses the plumbing, overflow tank, and calibration laser. The detector is located ~ 500 m from the Booster neutrino source.

The neutrino beam, produced using 8 GeV protons from the Booster at Fermilab, consists of a 70 cm Be target within a magnetic-horn focusing system, followed by a 50 m long pion decay volume. The proton beam is delivered to the experiment at a rate of up to 5 Hz and an intensity of $\sim 4 \times 10^{12}$ per spill, corresponding to an average current of about $3 \mu\text{A}$. Each spill is made up of 84 buckets of beam coming every 18.8 ns for a total duration of $1.6 \mu\text{s}$. The Booster can reliably deliver protons for about two-thirds of a calendar year, which allows the experiment to receive up to $\sim 5 \times 10^{20}$ protons per year.

The magnetic horn focuses secondary pions and kaons from the primary interactions and, as shown in Fig. 14, is made of Al and operates at a current of 170 kA, a voltage of 2.5 kV, and a pulse duration of $140 \mu\text{s}$. The high current flows along the inner conductor and back along the outer conductor, producing a toroidal magnetic field that focuses π^+ and defocuses π^- (or focuses π^- and defocuses π^+). Therefore, a fairly pure ν_μ or $\bar{\nu}_\mu$ beam can be produced, depending on the horn polarity. Fig. 15 shows the shape of the expected neutrino fluxes at the location of the detector.

An intermediate absorber can be lowered halfway down the decay pipe to change the decay path from 50 m to 25 m. The ability to take data at two decay distances allows a systematic check of the signal and backgrounds, as they have different dependences on distance. The ν_e background from μ^+ decay, for example, is concentrated at the downstream end of the decay pipe, while the ν_e background from K^+ decay is

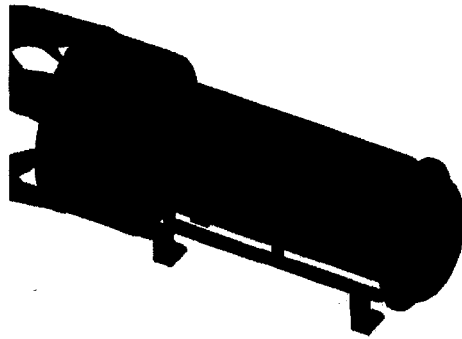


Figure 14: A schematic drawing of the MiniBooNE magnetic focusing-horn.

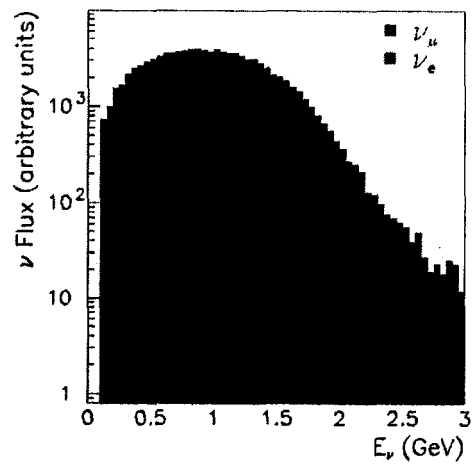


Figure 15: The shape of the expected MiniBooNE neutrino fluxes at the location of the detector.

Table 7: The approximate MiniBooNE number of signal and background events after 2 years (10^{21} protons on target) of data taking with neutrinos.

Process	Reaction	Number of Events
$\nu_\mu \rightarrow \nu_e$ Signal	$\nu_e C \rightarrow e^- X$	1000
Intrinsic ν_e Background	$\nu_e C \rightarrow e^- X$	1500
Mis-ID μ^- Background	$\nu_\mu C \rightarrow \mu^- X$	500
Mis-ID π^0 Background	$\nu_\mu C \rightarrow \nu_\mu \pi^0 X$	500

concentrated at the upstream end.

5.2. Neutrino Oscillation Signal and Background Reactions

Table 7 shows the approximate number of signal and background events after 2 full years (10^{21} protons on target) of data taking with neutrinos. If MiniBooNE verifies the LSND signal, then from $\nu_\mu \rightarrow \nu_e$ oscillations, approximately 1000 $\nu_e C \rightarrow e^- X$ events should be observed above background. There are 3 main backgrounds to the oscillation search: intrinsic ν_e background in the beam from μ and K decay in the decay pipe, mis-id μ events ($\nu_\mu C \rightarrow \mu^- X$), and mis-id π^0 events ($\nu_\mu C \rightarrow \nu_\mu \pi^0 X$). The total intrinsic ν_e background is estimated to be about 1500 events and will be determined from the measured rate of $\nu_\mu C \rightarrow \mu^- X$ events (for $\mu^+ \rightarrow e^+ \bar{\nu}_\mu \nu_e$ decays) and from the measured wide-angle muons in the LMC (for $K^+ \rightarrow \pi^0 e^+ \nu_e$ decays). The LMC is a telescope at a wide angle to the beam that measures the high-transverse momentum muons from K decay. The mis-id μ event background is estimated to be about 500 events and will be determined from the Michel-electron tag. (Note that 92% of the μ^- and 100% of the μ^+ decay in mineral oil.) Finally, the mis-id π^0 event background, which occurs when the π^0 decays asymmetrically, is estimated from the symmetric π^0 decays. Fig. 16 shows the expected signal and background energy distributions for the case of $\Delta m^2 = 0.4 \text{ eV}^2$ and $\sin^2 2\theta = 0.04$, while Fig. 17 shows the expected oscillation sensitivity for 2 years of ν_μ or $\bar{\nu}_\mu$ running.

5.3. Status Report

The MiniBooNE detector and beam are now fully operational, and data taking is going smoothly. The detector has been calibrated with laser-calibration events, the energy scale and resolution have been determined from cosmic-muon and Michel-electron events, and approximately 50,000 clean neutrino events have been recorded after the first six months of data taking with about 5×10^{19} protons on target. At present, the experiment is clearly reconstructing both $\nu_\mu C \rightarrow \mu^- X$ charged-current events and $\nu_\mu C \rightarrow \nu_\mu \pi^0 X$ neutral-current events, which are the two main backgrounds to the $\nu_\mu \rightarrow \nu_e$ oscillation search. Fig. 18 shows that events are peaked, as expected, along the neutrino beam direction, and as shown in Fig. 19, π^0 events are being reconstructed at approximately the correct mass with a mass resolution of about 23

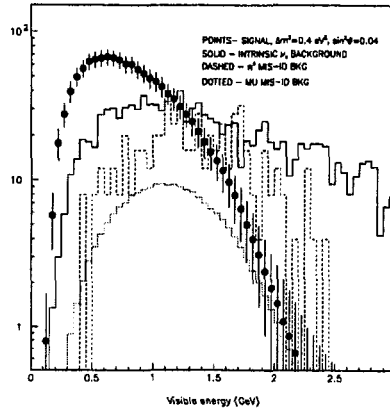


Figure 16: The MiniBooNE expected signal and background energy distributions for the case of $\Delta m^2 = 0.4 \text{ eV}^2$ and $\sin^2 2\theta = 0.04$.

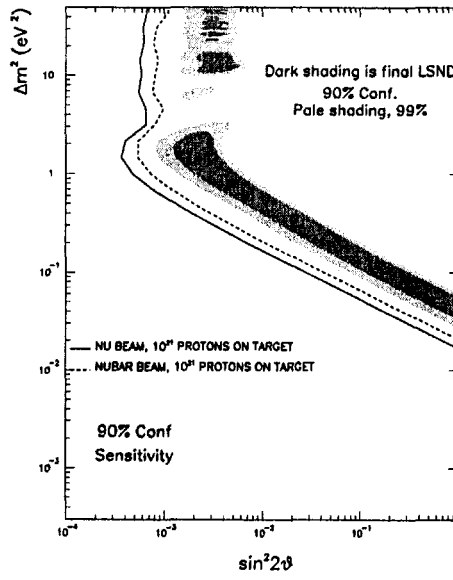


Figure 17: The MiniBooNE expected oscillation sensitivity for 2 years of ν_μ or $\bar{\nu}_\mu$ running.

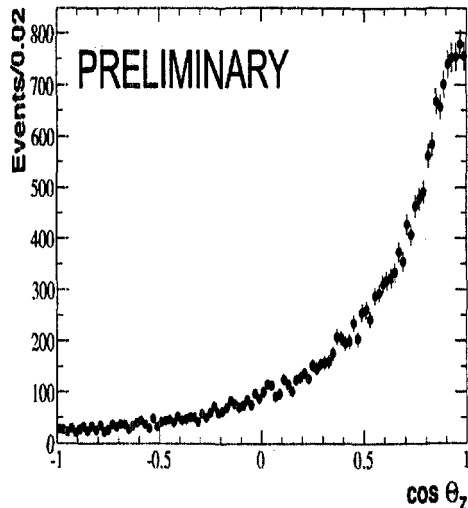


Figure 18: The MiniBooNE reconstructed $\cos\theta$ distribution for events that satisfy a simple selection criteria, where θ is the angle between the beam direction and the reconstructed event direction. As expected, event directions are peaked along the beam direction.

MeV.

The current plan is to run the first full year (5×10^{20} protons on target) with ν_μ and then switch to $\bar{\nu}_\mu$ running and 25 m absorber running. The future MiniBooNE schedule is dependent on the number of protons delivered per year to the experiment. First results are expected by 2005, and if the LSND oscillation signal is confirmed, an initial determination of the oscillation parameters can be made. A second detector (BooNE) will then be built at a different distance in order to obtain the highest precision measurement of the oscillation parameters. The neutrino flux goes as r^{-2} to very good approximation, so that a simple ratio of events in the two detectors as a function of energy will cancel most of the systematic uncertainties and will allow Δm^2 to be measured to $\pm 0.02 \text{ eV}^2$.

6. Conclusions

The confirmation of ν oscillations at high Δm^2 ($\Delta m^2 > 0.1 \text{ eV}^2$) would have a huge impact on astrophysics, as well as particle and nuclear physics. A joint analysis of the LSND and KARMEN experiments reveals compatible neutrino oscillation regions in a band from 0.2 to 1 eV^2 and in a region around 7 eV^2 . The MiniBooNE experiment at Fermilab will provide a definitive test of this evidence for high Δm^2 neutrino oscillations.

7. Acknowledgments

This work was made possible by the dedicated efforts of the LSND, KARMEN,

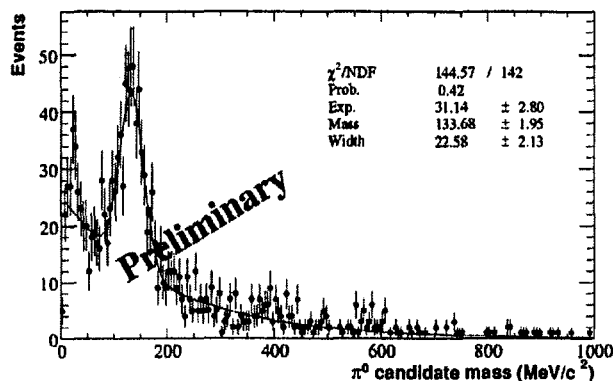


Figure 19: The MiniBooNE reconstructed π^0 mass distribution for events that satisfy a simple selection criteria. π^0 events are being reconstructed at approximately the correct mass with a mass resolution of about 23 MeV.

and MiniBooNE collaborations.

8. References

- 1) The MiniBooNE Collaboration consists of scientists from the following institutions: University of Alabama; Bucknell University; University of Cincinnati; University of Colorado; Columbia University; Embry-Riddle Aeronautical University; Fermi National Accelerator Laboratory; Indiana University; Los Alamos National Laboratory; Louisiana State University; University of Michigan; and Princeton University. More information may be found at <http://www-boone.fnal.gov/>.
- 2) A. Aguilar *et al.*, *Phys. Rev.* **D64** (2001) 112007.
- 3) B. Armbruster *et al.*, *Phys. Rev.* **D65** (2002) 112001.
- 4) E. D. Church, K. Eitel, G. B. Mills, and M. Steidl, *Phys. Rev.* **D66** (2002) 013001.
- 5) E. Church *et al.*, "A proposal for an experiment to measure $\nu_\mu \rightarrow \nu_e$ oscillations and ν_μ disappearance at the Fermilab Booster: BooNE", LA-UR-98-352, Fermilab experiment 898; A. O. Bazarko, *Nucl. Phys.* **B91** (Proc. Suppl.) (2001) 210.
- 6) C. Athanassopoulos *et al.*, *Nucl. Instrum. Methods* **A388** (1997) 149.
- 7) R. L. Burman, M. E. Potter, and E. S. Smith, *Nucl. Instrum. Methods* **A291** (1990) 621; R. L. Burman, A. C. Dodd, and P. Plischke, *Nucl. Instrum. Methods in Phys. Research* **A368** (1996) 416.

- 8) R. A. Reeder *et al.*, *Nucl. Instrum. Methods* **A334** (1993) 353.
- 9) J. J. Napolitano *et al.*, *Nucl. Instrum. Methods* **A274** (1989) 152.
- 10) This background also includes contributions from $\bar{\nu}_\mu C \rightarrow \mu^+ n X$ and $\nu_\mu C \rightarrow \mu^- n X$.
- 11) C. Athanassopoulos *et al.*, *Phys. Rev. C* **54** (1996) 2685; C. Athanassopoulos *et al.*, *Phys. Rev. Lett.* **77** (1996) 3082.
- 12) B. Achkar *et al.*, *Nucl. Phys.* **B434** (1995) 503.
- 13) G. Drexlin *et al.*, *Nucl. Instrum. Methods* **A289**, (1990) 490.
- 14) G. J. Feldman and R. D. Cousins, *Phys. Rev.* **D57** (1998) 3873.